Lab on a Chip

Cite this: *Lab Chip*, 2012, **12**, 852

www.rsc.org/loc

FOCUS

Acoustofluidics 6: Experimental characterization of ultrasonic particle manipulation devices

Jürg Dual,* Philipp Hahn, Ivo Leibacher, Dirk Möller and Thomas Schwarz

DOI: 10.1039/c2lc21067c

Because of uncertainties in material and geometrical parameters in ultrasonic devices, experimental characterization is an indispensable part in their successful application for the manipulation of particles or cells. Its miniaturized size precludes the use of many of the usual tools used for macroscopic systems. Also, a further challenge is the fact that the resulting motion due to the electromechanical actuation has both high frequency and small amplitudes. Contactless methods like laser interferometry are therefore promising methods. In addition, as long as there is strong electromechanical coupling between the transducer and the device also electrical measurements like admittance curves give insight into the frequencies at which the devices might work best. This is the case for example for piezoelectric transducers working at one of their resonance frequencies. Because the devices usually are used in resonant modes, narrow frequency detection methods like lock in amplifiers help to improve the signal to noise ratio. Also many analysis tools have been established in the context of modal analysis, which is based on frequency domain methods. Special emphasis is placed here on the determination of the quality factor Q of the resonator, as Q determines the efficiency of a device.

Institute of Mechanical Systems, Department of Mechanical and Process Engineering, ETH Zentrum, CH-8092 Zurich, Switzerland. E-mail: dual@imes.mavt.ethz.ch

A Introduction

Ultrasonic particle manipulation devices in lab on chip systems typically work at frequencies from 0.1 to 10 MHz given their typical size. They are usually quite complicated systems, consisting of a fluid volume containing particles, a solid bounding the fluid volume and transducers attached to the device either permanently or in a removable way. The transducers are piezoelectric devices[1–4] or have interdigitated transducers (IDTs).[5] Due to the complexity of the devices and scatter in their parameters (*e.g.* material properties or geometrical parameters including the thickness of glue layers), as well as temperature dependence of their properties, the modeling has its limitations, resulting in the need to characterize the devices nondestructively after assembly. When characterizing devices used for ultrasonic manipulation, a number of techniques are valuable, among others:

- admittance curves
- laser interferometry
- modal analysis
- microscopy
- particle image velocimetry (PIV).

In this tutorial the focus is put on laser interferometry, admittance curves and modal analysis exemplified by several examples.

When a device is in use for manipulation, microscopy, possibly in combination with particle image velocimetry, is an additional useful tool.[6,7]

B Laser interferometry

Laser interferometry is a powerful tool, when displacements or velocities on surfaces need to be measured on small devices, because it is a contactless measurement technique. Therefore, the measurement does not disturb the motion to be measured.

The propagation of light is described by Maxwell's equations.[8] Light propagates with the wave speed $c = 2.998 \times 10^8$ m s^{-1} in vacuum. The frequency f of the visible light ranges from about 4.0×10^{14} Hz to

Foreword

Characterization of your device is of major importance in order to build a successful acoustofluidic device. In this sixth paper of 23 in the tutorial series on Acoustofluidics in *Lab on a Chip*, Jürg Dual, Philipp Hahn, Ivo Leibacher, Dirk Möller and Thomas Schwarz describe methods to characterize resonant systems designed for ultrasonic particle manipulation, such as laser interferometry and modal analysis. Examples of transducer characterization with Q-factor determination and admittance measurements and simulations for planar resonator devices are presented. It is further shown how the complexity of the resonances in the system increases as a fluid layer is introduced in the resonator.

Andreas Lenshof – coordinator of the Acoustofluidics series.

7.9×10^{14} Hz, resulting in a wavelength $\lambda = c/f$ from about 380 nm to 750 nm.

A linearly polarized plane harmonic light wave (*e.g.* from a laser with sufficiently long coherence length) propagating in the direction of $\boldsymbol{e}_z$ is described with respect to an orthonormal xyz coordinate system by:

$$\boldsymbol{E} = E_y\boldsymbol{e}_y = A\cos(\omega t - kz)\boldsymbol{e}_y, \qquad (1)$$

where $\boldsymbol{E}$ is the electrical field, A is the amplitude, $\omega = 2\pi f$ is the angular frequency and $k = \omega/c$ is the wavenumber.

The frequency of the visible light is too high to be detected directly, therefore detectors are used that measure the time averaged energy flux, the intensity I, which is given by:

$$I = c\varepsilon_0 \frac{1}{T}\int_T \boldsymbol{E}\cdot\boldsymbol{E}\,\mathrm{d}t = c\varepsilon_0\langle \boldsymbol{E}\cdot\boldsymbol{E}\rangle, \qquad (2)$$

where ε_0 is the vacuum permittivity, T is the period of the wave and $\langle\ \rangle$ denotes the time average. The factor $c\varepsilon_0$ will be omitted in the following.

Various types of interferometers exist.[9] In the most common setup used for particle manipulation, the light energy from a laser is split into two beams using a beam splitter, one of which is called the reference beam and the other is called the object beam.

The reference beam is reflected from a fixed mirror, while the object beam is reflected from the surface moving with displacement $u(t)$ in the direction of the object beam. If the two beams $\boldsymbol{E}_1$ and $\boldsymbol{E}_2$ are recombined and superposed, *i.e.* interfere with each other, the resulting intensity is:

$$I = \langle \boldsymbol{E}_1^2\rangle + \langle \boldsymbol{E}_2^2\rangle + 2\langle \boldsymbol{E}_1\cdot\boldsymbol{E}_2\rangle, \qquad (3)$$

where the last term is the phase-dependent interference term. At the detector, assuming that the two fields have the same polarization and propagation directions one obtains for the total intensity:

$$I = I_1 + I_2 + \sqrt{I_1 I_2}\cos\delta, \qquad (4)$$

where $\delta = k(\Delta z - 2u(t))$ and I_i is the intensity of beam i.

The (static) difference in path length of the two beams is Δz. Therefore the intensity varies between a minimum ($\delta = (2N-1)\pi$) and a maximum ($\delta = 2N\pi$), depending on the phase difference δ between the two waves. N is an integer number. If u changes with time, the intensity varies with time. This intensity variation is detected with a photodiode.

In order to discriminate between motion towards and motion away from the laser as well as to improve the signal to noise ratio, often a process called heterodyning is used, where one of the beams is shifted in frequency with respect to the other *e.g.* using an acousto-optic modulator. Upon interference the voltage signal at the photodetector then has a carrier frequency f_C (typically about 100 MHz) equal to the difference in frequencies $(f_2 - f_1)$ of the two beams.

$$I(t) = \frac{1}{T}\int_T A_1^2\cos^2[2\pi f_1 t] + A_2^2\cos^2[2\pi f_2 t + \delta] + A_1A_2\{\cos[2\pi(f_2 - f_1)t + \delta] + \cos[2\pi(f_2 + f_1)t + \delta]\}\mathrm{d}t. \qquad (5)$$

Because of the low pass behavior of the photodetector, the first two terms are

Jürg Dual

Jürg Dual has been a Full Professor of Mechanics and Experimental Dynamics in the Center of Mechanics of the Institute of Mechanical Systems at the ETH in Zurich since October 1, 1998. Since 2008 he also has been the President of the University Assembly of ETH in Zurich. Jürg Dual studied mechanical engineering at the ETH Zurich. He then spent two years on a Fulbright grant at the University of California in Berkeley, where he graduated with an MS and an MEng degree in mechanical engineering. He then received his Dr Sc. Techn. degree at the ETH Zurich. After one year as a visiting assistant professor at Cornell University, Ithaca, NY, he returned to the ETH Zurich as an assistant professor. He is a Fellow of the ASME, member of the SATW (Swiss Academy of Technical Sciences) and Honorary Member of the German Association for Materials Research and Testing. His research focuses on wave propagation and vibrations in solids as well as micro- and nano-system technology.

Philipp Hahn

Philipp Hahn received the MSc degree in mechanical engineering from the University of Wisconsin at Madison in 2009. During his studies he focused on computational mechanics and precision engineering. In Spring 2010 he was a research intern at NASA JPL, working on granular dynamic simulations. He is currently pursuing the PhD degree at the Institute of Mechanical Systems, ETH Zurich where his main research area is ultrasonic manipulation.

Ivo Leibacher

Ivo Leibacher graduated in 2010 with an MSc in mechanical engineering at the Swiss Federal Institute of Technology (ETH Zurich), where he is currently a PhD student at the Institute of Mechanical Systems. For his master thesis, he worked on the temperature control of a microfluidic sensor, and after a work experience in medical engineering he is now focusing on the applications of ultrasonic manipulation within microfluidic devices.

averaged to yield a DC voltage V_0. The term with the sum of the frequencies will average to zero, while the term with the frequency difference will yield the signal to be demodulated.

$$V(t) = V_0 + K A_1 A_2 \cos\left[2\pi(f_2 - f_1)t + \frac{2\pi}{\lambda}(\Delta z - 2u(t))\right], \quad (6)$$

where K is a constant. Eqn (6) describes a phase modulated signal with carrier frequency $f_C = f_2 - f_1$.

Alternatively, this can be interpreted as a frequency modulated signal according to:

$$\dot{\phi}(t) = 2\pi f^*(t), \quad (7)$$

where ϕ and f^* are instantaneous phase and frequency of the signal.

Combining with eqn (6) one obtains

$$\dot{\phi} = 2\pi f_C - \frac{4\pi}{\lambda}\dot{u} = 2\pi(f_C - f_D), \quad (8)$$

where $f_D(t) = 2\dot{u}/\lambda$ is the Doppler frequency. The frequency modulated signal is then written as:

$$V(t) = V_0 + KA_1A_2\cos[2\pi(f_C - f_D)t]. \quad (9)$$

Accordingly, eqn (6) and (9) are demodulated using:

- fringe counting or phase demodulation to yield displacement and
- frequency demodulation to yield velocity, respectively.

Displacement amplitudes in ultrasonic manipulation devices are often much less than the wavelength, typically of the order of 10 nanometers. Fringe counting is therefore less suitable than phase demodulation. However, low frequency motions (caused by thermal drift, shocks, *etc.*) must be eliminated. For this purpose the reference mirror can be mounted on a piezoelectric element (for low frequency path length stabilization) or its influence on the signal is eliminated in the demodulation process.[10] Commercial phase demodulators have a frequency range up to about 20 MHz, with a maximum displacement of about $\lambda/8$, which is about 80 nm for a typical HeNe laser. Corresponding velocity decoders have slightly lower frequency range and are suitable up to similar amplitudes.

When the structure to be investigated is very small, the object beam needs to be precisely focused. This is best done with a fiber optic interferometer, where a spot size of <5 μm can be obtained. When both arms of such an interferometer are reflected at different points on the object, the difference of the displacements or velocities is measured.

In-plane displacements can also be measured, *e.g.* using a Bauernfeind prism rotating about the optical axis. Because here the light needs to be retro-reflected, a special tape or paint is used on the surface. However, this might not be possible without affecting the motion, if the structures are very small, because of the additional mass loading.

Obtainable resolution in interferometry

When comparing different interferometer systems, the SNR (signal to noise ratio) and the frequency range are crucial. The theoretical maximum resolution is limited by shot noise at the detector.

As a measure for the resolution one can take the displacement for SNR = 1. In general, it is given by[11]

$$u_{\min} = k\sqrt{\frac{\Delta\tilde{f}}{\eta P_0}} \quad (10)$$

where η is the detector efficiency (*e.g.* 10%), P_0 is the laser power (*e.g.* 1 mW), $\Delta\tilde{f}$ is the bandwidth used in the measurement and k is a constant, depending on the configuration of the optical setup.

A typical value is:

$$u_{\min}/\sqrt{\Delta\tilde{f}} = 10^{-14}\mathrm{m}/\sqrt{\mathrm{Hz}}. \quad (11)$$

For a bandwidth $\Delta\tilde{f}$ = 1 MHz one can therefore expect a maximum resolution of 10^{-11} m. By limiting the bandwidth or averaging n times, the resolution can be further improved according to the $1/\sqrt{n}$ law, where n is the number of averages.

C Frequency analysis, admittance curves and modal analysis

The ultrasonic manipulation system without the particles is usually assumed to be linear and time invariant. Therefore, the tools available from linear systems analysis are applicable. In particular, the system excited with one frequency will have a stationary solution with a motion of the same frequency (Fig. 1).

In order to determine the system properties, one can either excite the system harmonically with an excitation $x(t)$ and scan the excitation frequency through the range of interest.

Dirk Möller

Dirk Möller received the MSc degree in mechanical engineering from the Swiss Federal Institute of Technology, Zurich, in 2007, where he is currently pursuing the PhD degree at the Center of Mechanics. During his studies he focused on micro- and nanosystems. His main research area is ultrasonic manipulation within microfluidic devices.

Thomas Schwarz

Thomas Schwarz received the MSc degree in electrical engineering from the Dresden University of Technology in 2007. He is currently pursuing the PhD degree at the Institute of Mechanical Systems, ETH Zurich. During his studies he focused on precision and microengineering. Currently, his main research area is ultrasonic manipulation within microfluidic systems.

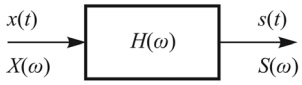

Fig. 1 Linear system, characterized by the transfer function $H(\omega)$ with input $x(t)$ and output $s(t)$ and corresponding spectra $X(\omega)$ and $S(\omega)$.

Alternatively, repetitive broad band spectra can be used as excitation, for example a linear sweep signal or band limited white noise. Then the Fourier transform[12] can be applied to both excitation and measured signal, resulting in the corresponding spectra. For measurement data, the signals first need to be digitized, then the discrete Fourier transform is applied using the FFT algorithm to yield the desired spectra. A detailed analysis of the discrete Fourier transform and its comparison with the continuous Fourier transform are given in ref. 13.

A general signal $x(t)$ discretized with sample frequency $f_s = 1/T$ (Fig. 2) will yield meaningful spectra up to the Nyquist frequency $f_N = \frac{1}{2}f_s$. This is the result of the sampling theorem. The maximum frequency in the signal therefore needs to be smaller than f_N, otherwise aliasing errors occur.[13] This is assured by using anti-aliasing analog filters before the sampling. Also, one should be aware that suitable windows need to be applied before the FFT in order to avoid leakage.[13] The frequency resolution of the result of the FFT will be given by $\Delta f = 1/T_0$, where T_0 is the length of the sample.

Referring to Fig. 1, in the frequency domain, the concept of the transfer function $H(\omega)$ is used, which is defined as:

$$H(\omega) = \frac{S(\omega)}{X(\omega)}. \tag{12}$$

where $H(\omega)$ is the quotient of the Fourier transforms of output $S(\omega)$ and input $X(\omega)$. The accuracy of the result can be assessed using the coherence function γ^2 (ref. 14), which is used to obtain confidence intervals. An estimate $\hat{\gamma}^2$ of the coherence function γ^2 can be gained from

$$\hat{\gamma}^2(\omega) = \frac{\overline{|S(\omega)X^*(\omega)|}}{\overline{X(\omega)X^*(\omega)}\ \overline{S(\omega)S^*(\omega)}}, \tag{13}$$

where the superposed bar denotes averaging over the number of samples and the superscript * means the complex conjugate. Without noise the coherence function equals 1. As soon as there is noise $\hat{\gamma}^2 < 1$. Bad coherence function values can be the result of many effects, *e.g.* bad signal to noise ratios at a particular frequency, undefined trigger levels, scatter in the excitation and others.

In order to understand the behavior of an ultrasonic manipulation system modal analysis is a widely used method. Using linear system analysis a structure is characterized dynamically in terms of its resonance frequencies, damping and modes of vibrations. For every device an infinite number of resonances exist. In many cases the lowest resonances are most important. For every mode, in principle the whole structure including the excitation is involved.

For ultrasonic manipulation devices, typically piezoelectric elements are used to excite the structure. Laser interferometers are used to determine the mechanical response. If the mode shapes are also important, then the structure can be scanned in 1D or 2D with a laser interferometer, which might be a challenge; if the structure is small, however, it can give detailed information about displacement distributions.

If only the resonance frequencies and their damping are needed, in principle it is sufficient to measure the transfer function between excitation at one position and response at another position. If neither of the two positions is a node of one of the resonance modes, all the frequencies and damping values can be found.

When the damping of the mode is not too large and the electromechanical coupling is strong (*e.g.* near a transducer resonance) admittance curves of the transducer can also be used to determine the resonance frequencies and damping.[15] The electrical admittance Y is a measure of how easily an element will allow an electrical current to flow and is defined as:

$$Y = \frac{1}{Z} = G + iB \tag{14}$$

where Z is the impedance, G is the conductance and B is the susceptance. All are functions of frequency.

If the resonance modes are separated enough (depending on damping) one can decouple the modes and consider them as single degree of freedom oscillators with modal coordinate s_j and modal excitation $\bar{f}_j$. This also corresponds to the modal decomposition in a FEM analysis.[16,17] The differential equation describing mode j is

$$m_j\ddot{s}_j + \delta_j\dot{s}_j + k_j s_j = \bar{f}_j, \tag{15}$$

where m_j, δ_j and k_j are the modal mass, damping and spring constant of mode j, respectively. The resonance frequency is given by

$$\omega_{0j} = \sqrt{\frac{k_j}{m_j}}, \tag{16}$$

and the transfer function H_j for harmonic excitation by

$$H_j = \frac{s_j}{\bar{f}_j} = \frac{1}{m_j}\frac{1}{\omega_{0j}^2 - \omega^2 + i\omega\delta_j/m_j}. \tag{17}$$

Using partial fractions one obtains:

$$H_j = \frac{1}{2i\omega_{0j}m_j}\left(\frac{1}{i\omega + \lambda_j} - \frac{1}{i\omega + \lambda_j^*}\right), \tag{18}$$

where

$$\begin{aligned} \lambda_j &= \frac{\delta_j}{2m_j} - i\omega_{0j}, \\ \lambda_j^* &= \frac{\delta_j}{2m_j} + i\omega_{0j}. \end{aligned} \tag{19}$$

For positive ω and damping which is not too large, the first term in eqn. (18) dominates in the vicinity of ω_0. If one neglects the second term and plots the

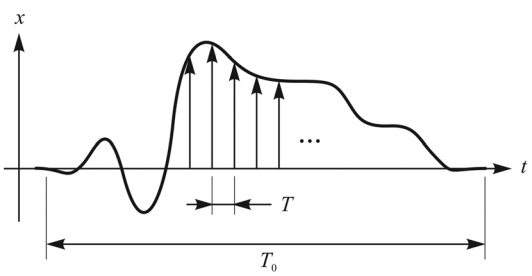

Fig. 2 A general voltage signal $x(t)$ is discretized with sampling frequency $f_s = 1/T$ for a sample length T_0. The arrows (not all are shown) represent the sampling points, which are equally distributed across the whole sample length T_0.

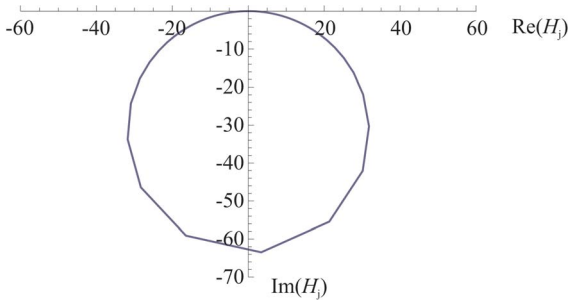

Fig. 3 Complex representation of the approximation of the transfer function $H_j(\omega)$ of mode j in the complex plane near a resonance frequency ω_{0j}. Please note the insufficient frequency resolution that might result from the application of the discrete Fourier transform, when the damping is low.

resulting $\mathrm{Re}(H_j)$ and $\mathrm{Im}(H_j)$ in the complex plane (Fig. 3), we obtain the equation of a circle, which can be used to fit the damping δ_j (ref. 17)

$$\mathrm{Re}(H_j)^2+\left(\mathrm{Im}(H_j)+\frac{1}{2\omega_{0j}\delta_j}\right)^2 = \left(\frac{1}{2\omega_{0j}\delta_j}\right)^2 \quad (20)$$

Also the quality factor Q_j can be defined for the respective mode j:

$$Q_j = \frac{m_j\omega_{0j}}{\delta_j} = \frac{\omega_{0j}}{\omega_{uj}-\omega_{lj}} = \frac{\omega_{0j}}{\Delta\omega_j}. \quad (21)$$

where ω_{uj} and ω_{lj} are the angular frequencies, which correspond to phase values of the phase at resonance +/− π/4. For $Q > 10$ these are also about equal to the frequencies, for which the amplitude is $1/\sqrt{2}$ of the maximum amplitude. Q is therefore given by the resonance frequency divided by the bandwidth.

The transfer function of the whole system can then be composed of the sum

$$H = H_1 + H_2 + H_3 + \ldots, \quad (22)$$

where each mode can have different parameters.

D Measurements

In the following section, measurements of the electrical and mechanical behavior of piezoelectrically driven systems are outlined. The understanding of the measured results is supported by comparison with simulation results. First, a simple piezoelectric element is characterized by admittance and interferometer measurements, then these methods are applied to several manipulation devices.

1. Characterization of a transducer

1.1. Experimental setup. The experimental setup for interferometer measurements is illustrated in Fig. 4. For the excitation of a piezoelectric element, a function generator (Stanford research systems, model DS345) is used in connection with a broadband power amplifier (ENI 2100L). For laser vibrometry, a Polytec OFV 303 sensor head is connected to a Polytec OFV 3001 vibrometer controller. The velocity measurement signal of the vibrometer is then connected to a LeCroy WaveSurfer™ 424 oscilloscope for further data analysis. The measurement and excitation signals are filtered by a low-pass filter (Krohn-Hite model 3945). For admittance measurements of piezo elements, an impedance analyzer (Sine Phase Z-Check 16777k) is used, which has a range of 1 kHz to 16.7 MHz. Another method for the admittance measurement has been reported in ref. 18: a current probe was connected to an oscilloscope and the current signal together with the voltage signal have been recorded and processed.

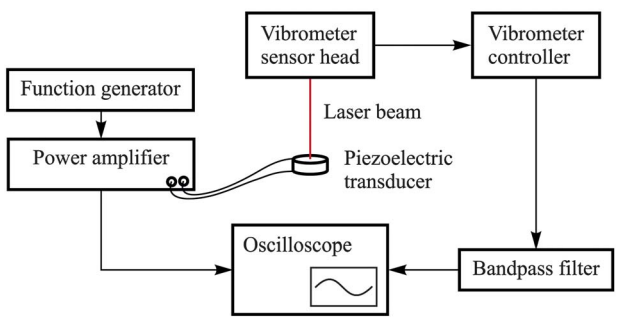

Fig. 4 Schematic illustration of the experimental setup for laser interferometry measurements of a piezoelectric transducer. The path of the analog excitation and measurement signals is marked by arrows.

1.2. Correlation between electrical and mechanical measurements. As a simple first example, the electrical properties of a piezoelectric transducer are compared to its mechanical behavior over a certain frequency range. A cylindrical piezoelectric element of diameter 6.3 mm and thickness 2.9 mm (PZ 27, Ferroperm Piezoceramics) with polarization direction along the cylindrical axis is chosen. The two electrodes at the top and bottom of the cylinder are electrically connected to wires, which also allow for a free mounting of the piezoelectric element.

The admittance curve of the described transducer is measured in a range from 50 kHz to 1.5 MHz. Its absolute value is plotted in Fig. 5a. Five major maxima peaks represent the transducer's resonance frequencies. In the following, the admittance and transfer function are studied.

For the mechanical characterization of the piezoelectric element, its transfer function $H(\omega) = S(\omega)/X(\omega)$ is calculated between the excitation voltage $X(\omega)$ of the piezoelectric transducer and the velocity amplitude $S(\omega)$ as measured by laser vibrometry. The laser beam is pointed at an electrode surface of the cylindrical piezoelectric element. In order to measure the vibration along the cylindrical axis of the piezoelectric element, the laser beam is adjusted to be parallel to this axis. An excitation over a large frequency range is desired, hence for $X(\omega)$ white noise is used. The chosen white noise signal has a root mean square (RMS) value of 23.6 V, which is high enough to obtain a sufficient coherence. Alternatively, a frequency sweep over a certain frequency range could also be applied.

A 10 ms time signal of both the excitation and the velocity measurement is recorded at 14 well-distributed random points on the top surface of the cylindrical

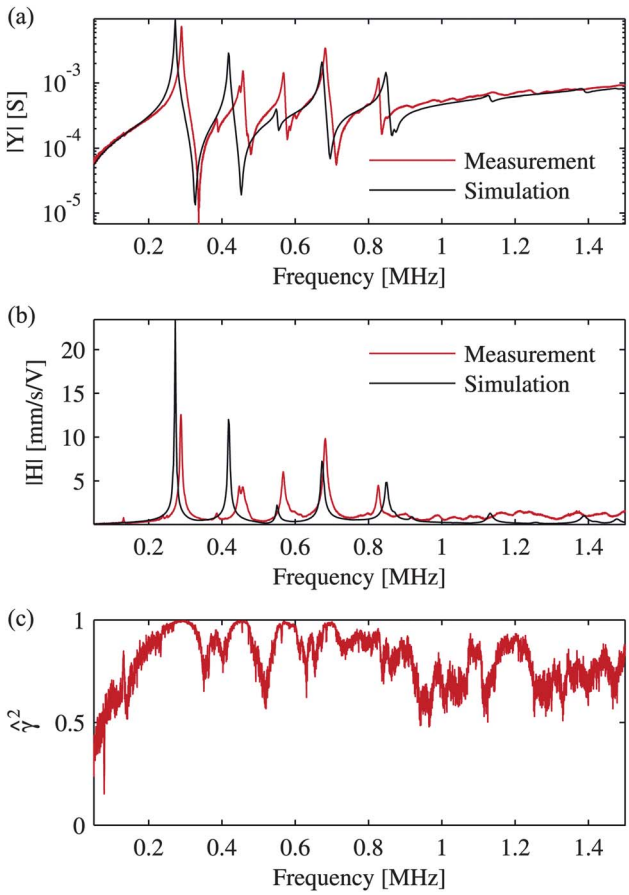

Fig. 5 Characterization of a piezoelectric element. (a) The absolute value of its admittance $|Y|$, (b) the absolute value of the transfer function $|H|$ as well as (c) the estimate of the coherence function $\hat{\gamma}^2$ are plotted against frequency. The comparison of admittance and transfer function reveals the coupling between these quantities, especially at the five clearly visible resonance peaks. For (b) and (c), a driving voltage with a RMS value of 23.6 V is applied in the experiment. Simulation results are also plotted in (a) and (b). In (c), a coherence close to 1 ascertains the quality of the measurement.

piezoelectric element. The measured maximum velocity, averaged over all measurement points, accounts for 149.2 mm s^{-1}, and the RMS value of the measured velocity is 41.0 mm s^{-1}, also averaged over all measured points. By means of a fast Fourier transformation (FFT), the measurement signal is transformed into the frequency domain with a resolution of 100 Hz. Low-pass filters with a cut-off frequency of 2 MHz are applied to avoid aliasing errors. In order to reduce the spectral leakage, the time signals are enveloped by Hamming windows before the FFT.[13]

In Fig. 5b, the resulting transfer function is plotted. Five major peaks can be observed in the plotted frequency range, which correspond to different resonant modes of the piezoelectric element. For the verification of the measurement quality, the estimate of the coherence $\hat{\gamma}^2$ between $S(\omega)$ and $X(\omega)$ is plotted in Fig. 5c. Especially around the resonance frequencies, a coherence close to 1 is observed, which underlines the validity of the measurement.

The five major peaks of the transfer function occur at the same resonance frequency as the five positive peaks in the transducer's admittance curve, revealing the electromechanical resonances. Whereas the five positive peaks in the admittance curve at resonance frequency result in a minimal impedance (series resonance), the corresponding proximate negative peaks with maximal impedance are known as the antiresonance (parallel resonance). The physical interpretation of the demonstrated relation between the admittance curve and the transfer function lies in the interplay between the inverse and the direct piezoelectric effect. The electromechanical coupling of the piezoelectric material can be seen as the conversion from electrical to mechanical energy and *vice versa*.

For a better understanding of the resonances, the piezoelectric element is also simulated in COMSOL Multiphysics® 4.1 with a finite element model. The piezoelectric material PZ27 is modeled with a density of $\rho = 7700\ \mathrm{kg\ m^{-3}}$ and a stiffness matrix with the components,[19] $c_{E11} = c_{E22} = 147$ GPa, $c_{E33} = 113$ GPa, $c_{E44} = c_{E55} = 23.0$ GPa, $c_{E66} = 21.2$ GPa, $c_{E12} = c_{E21} = 105$ GPa and $c_{E13} = c_{E23} = c_{E31} = c_{E32} = 93.7$ GPa, a coupling matrix with the components $e_{15} = e_{24} = 11.64\ \mathrm{C\ m^{-2}}$, $e_{31} = e_{32} = -3.09\ \mathrm{C\ m^{-2}}$, $e_{33} = 16.0\ \mathrm{C\ m^{-2}}$ and a complex relative permittivity $(1 - 0.017i)$ with the components $\varepsilon_{rS11} = \varepsilon_{rS22} = 1130$ and $\varepsilon_{rS33} = 914$.

Complex material parameters are set to yield a quality factor of $Q = 100$. The model allows evaluation of the current across electrodes for a given voltage, so the transducer's admittance can be calculated. The simulation results for the velocity amplitude and the admittance are also plotted in Fig. 5. However, in contrast to the measurements, the velocity amplitude was averaged over the whole top surface of the cylindrical piezoelectric element. Differences between the measurement and the simulation can be caused by material variations, the electrical wiring, noise in the electrical signal, as well as the different averaging.

The advantage of a simulation model lies in the more profound understanding of the resonant modes. For example, the resonance at about 0.68 MHz in the measurement corresponds to the resonance at 0.6725 MHz in the simulation. Its resonant mode can be identified as a thickness mode of the piezoelectric element as illustrated in Fig. 6. The three dimensional plot of the cylindrical transducer shows the z-component of the displacement field, whereas the z-axis is parallel to the axis of the cylinder. The displacement undergoes half a wavelength along the axis of the cylinder, where the highest amplitudes occur.

For the individual piezoelectric element as presented here, the electromechanical resonance frequencies were studied. When a piezoelectric element is attached to an ultrasonic particle manipulation device, the transfer function as well as the admittance curve will show many more

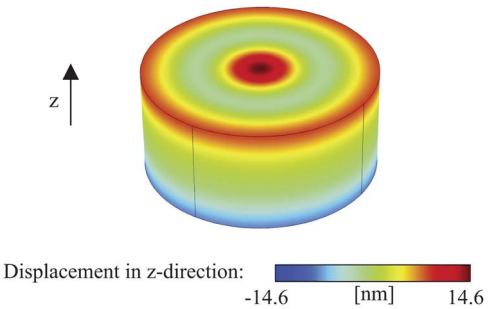

Fig. 6 In the simulated resonant mode, the displacement field in z-direction of the cylindrical piezoelectric transducer is shown. A harmonic excitation with an amplitude of 10 V was applied between the top and bottom electrodes at the resonance frequency of 672.5 kHz. The highest displacements are found on the axis of the cylinder.

resonance frequencies of the system, which are caused by additional structural resonance modes, as will be shown later.

1.3. *Q*-Factor. Different types of mechanical resonances are utilized in the field of ultrasonic particle manipulation. Resonances of the fluid cavity cause the radiation forces which are used for the particle manipulation, while transducer resonances are leveraged to enhance the amplitudes. Structural resonances of the enclosure are sometimes desired to couple with the fluid but they can as well disturb the standing pressure field in the fluid. All of these resonances combined lead to the complex patterns which can be observed in Fig. 13 and 15. The damping associated with each material can be expressed by a material quality factor or Q-factor.

In experiments, however, the energy transferred into the support of the device is another important factor that affects each resonance mode. This effect is frequency dependent since the rate at which the energy is transferred into the support strongly depends on the specific vibration pattern of the device. The electromechanical coupling of piezoelectric elements shows significant frequency dependent damping as well. Typically, low frequencies show higher damping.[21] Additionally, there exists a number of more complex damping mechanisms within the fluid. They can be traced back to streaming, to the radiation forces and to the scattering in the fluid–particle suspension. The combination between the material Q-factors and the other damping mechanisms damps each resonance of a manipulation device, leading to well defined peaks, each with a specific bandwidth and magnitude. Due to the frequency dependent components of the damping, both parameters not only depend on the material damping, but also depend on the specific resonance mode. Even if the system consists of only one material, as is the case in Fig. 4, the resonance peaks will still display individual bandwidths and magnitudes. In order to characterize each resonance peak, the total Q-factor is used.[16]

Material Q-factors are of primary interest for the use in simulations. Here, the attainable pressure amplitudes in the fluid strongly depend on them. Furthermore, the relation between the material Q-factors for the fluid and the solid device components defines how strongly structural resonances can affect the standing pressure field in the fluid. In contrast to material Q-factors, the Q-factors defined for each resonance are rather of practical importance. Particle manipulation devices that use one specific resonance have an operating frequency range which strongly depends on the Q-factor of the resonance. Moreover, strong standing pressure fields can be expected only for high resonance peaks, typically the ones with a high Q-factor.

As compared to material Q-factors which are widely available in the literature, the Q-factors corresponding to a specific resonance mode need to be determined either in simulations or in experiments.

In order to demonstrate different methods, the Q-factor of one resonance is determined on the basis of the admittance curve and the transfer function, measured in Section 1.2. As an example, the thickness mode of the piezoelectric element at a frequency of around 0.68 MHz is chosen. It is important to note that the demonstrated techniques only work for strong and distinct resonance peaks that can clearly be separated from each other. This becomes a problem for complex devices with a vast number of resonances (compare Fig. 15).

The Q-factor of a resonance can be deduced from measurements by means of various methods. Here, only the most common techniques are demonstrated, starting with those for the admittance curve. In order to minimize the error, all of them require resonance peaks which display a resonance–antiresonance attenuation difference of at least 25 dB. If this ratio is smaller, the error steeply increases up to invalid values at around 10 dB. More sophisticated methods exist which can be used for weak resonances; however, these methods are beyond the scope of this tutorial.[21]

The resonance–antiresonance attenuation difference is illustrated in Fig. 7 between the maximum and the minimum of the absolute admittance curve $|Y|$. The chosen peak leads to a ratio of $A = 36$ dB which is well in the range where the classical techniques provide accurate results. As mentioned in Section C, the Q-factor can be calculated by dividing the resonance frequency f_0 by the bandwidth Δf of the resonance peak. The bandwidth is generally given as the difference between an upper frequency f_u and a lower frequency f_l.

$$Q = \frac{f_0}{\Delta f} = \frac{f_0}{f_u - f_l} \tag{23}$$

The resonance frequency $f_0 = 681.5$ kHz can be found at the point of maximum conductance G in Fig. 7. Also illustrated in Fig. 7 and 8 are three different ways of how f_u and f_l can be found. The first option is to choose the frequencies at which the conductance reaches a level ½ or −6 dB of its maximum value ($f_{u(-6dB)}$ and $f_{l(-6dB)}$). The second option is to choose the frequencies corresponding to the susceptance extremes ($f_{u(s)}$ and $f_{l(s)}$). Finally, the third option is to choose the frequencies in the phase plot (see Fig. 8) which have a phase shift of ±45° relative to the resonance frequency ($f_{u(\pm 45°)}$ and $f_{l(\pm 45°)}$). All specific frequency values are shown in Table 1 together with the corresponding Q-factors.

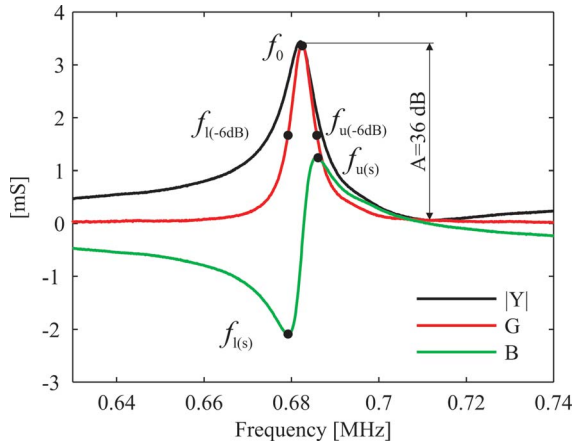

Fig. 7 Q-Factor determination using the admittance curve. As an example a thickness mode of a piezoelectric element without mechanical load is measured. The absolute value of the admittance Y is already shown in Fig. 5a. The upper and lower frequencies f_u and f_l can be evaluated using the conductance G and the susceptance B.

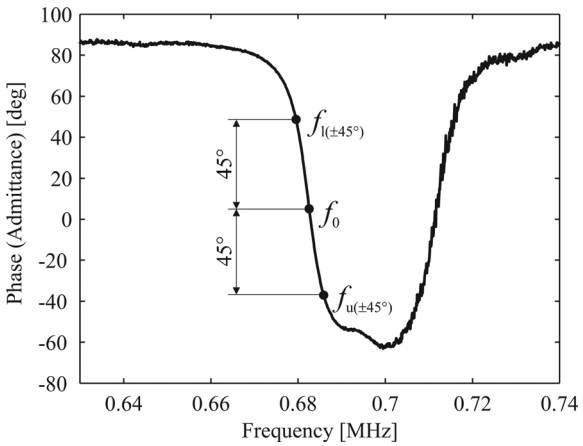

Fig. 8 Q-Factor determination at the example of a thickness mode of a piezoelectric element using the phase plot corresponding to the admittance measurement. The upper and lower frequencies f_u and f_l can be found at the phases of $\pm45°$ relative to the resonance frequency f_0.

For a physical interpretation of the different components in the admittance plot in Fig. 7 it is useful to consider two basic relations. First, the current is the product of the applied voltage and the admittance. This leads to the conclusion that the part of the current which is in phase with the applied voltage at a certain frequency is proportional to the conductance G. Second, the converted power is the product of the applied voltage and the part of the current which is in phase with the latter. In this sense, the conductance is a measure of the converted power. Of course, not all of the electrical power is converted into mechanical power because a part is transferred into heat. A similar interpretation could follow for the susceptance B. However, the information of both conductance and susceptance can also be visualized more intuitively in the form of an absolute value $|Y|$ and a phase as demonstrated in Fig. 7 and 8. The absolute value is then a measure of the absolute current while the angle between the applied voltage and the current is given by the phase.

The Q-factor of the resonance can also be deduced from the velocity transfer function. This might be the more intuitive choice, however, compared to admittance measurements it requires more expensive equipment. Additionally, in some cases measurements might not even be possible if the frequencies exceed the frequency range of the measurement equipment or if the velocity amplitudes are simply too low.

The resonance frequency $f_0 = 681.2$ kHz is obtained from Fig. 9 at the maximum of the magnitude of the transfer function $|H|$. The frequency is slightly different from the one obtained using the admittance curve. However, the difference is usually very small. Typically, two methods can be used to deduce f_u and f_l from the transfer function. The points at which the absolute value of the transfer function reaches a level of $1/\sqrt{2}$ or -3 dB of its maximum value are marked in Fig. 9. The points with a phase shift of $\pm45°$ relative to the resonance frequency can be seen in Fig. 10.

All specific frequency values are shown in Table 2 together with the corresponding Q-factors.

The physical interpretation of the real and complex components of the transfer function H in Fig. 9 is not an easy task since the physical effects involved in the transfer of the electrical input voltage to the mechanical output velocity are quite complicated. For this reason it is more useful to consider only the absolute value of the transfer function which relates to the sensitivity of the system and the phase which gives the angular relation between the input voltage and the output velocity.

The Q-factor can also be calculated from the time constant τ obtained by measuring the decaying velocity amplitude after a monochromatic resonant excitation is turned off. However, for high-Q systems, this method is very error prone because a slight deviation from the exact resonant frequency results in drastically reduced Q-factors. Additionally, abruptly switching off the excitation might excite other resonances of the system which also increases the error. Nevertheless, this method provides an

Table 1 The different upper and lower frequencies f_u and f_l, obtained from the admittance measurement in Fig. 7 and 8 and the resulting Q-factor. Since the three different ways of measuring the Q-factor are based on the same assumptions, the differences are due to measurement errors

f_0	681.5 kHz	
$f_{l(-6dB)}$	678.2 kHz	$Q = 103$
$f_{u(-6dB)}$	684.8 kHz	
$f_{l(s)}$	678.2 kHz	$Q = 105$
$f_{u(s)}$	684.7 kHz	
$f_{l(\pm45°)}$	678.3 kHz	$Q = 99$
$f_{u(\pm45°)}$	685.2 kHz	

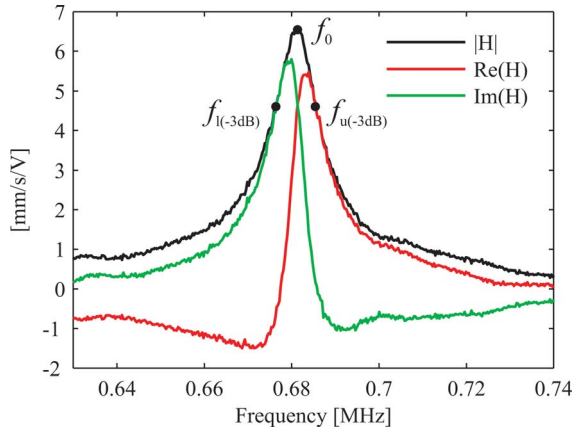

Fig. 9 Q-factor determination at the example of a thickness mode of a piezoelectric element without mechanical load using the transfer function H. The magnitude of the transfer function $|H|$ is already shown in Fig. 5b. The upper and lower frequencies f_u and f_l can be found from the magnitude at a level of −3 dB relative to the resonance frequency f_0.

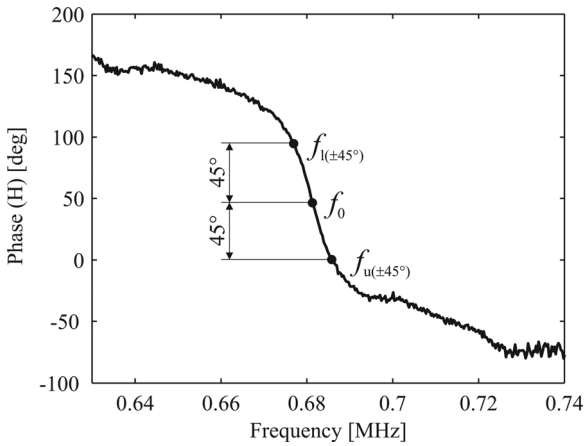

Fig. 10 Q-factor determination at the example of a thickness mode of a piezoelectric element using the phase plot of the transfer function H. The upper and lower frequencies f_u and f_l can be found at the phases of ±45° relative to the resonance frequency f_0.

Table 2 The different upper and lower frequencies f_u and f_l, obtained from the measured transfer function in Fig. 9 and 10 and the resulting Q-factor

f_0	681.2 kHz	
$f_{l(-3dB)}$	676.6 kHz	$Q = 77$
$f_{u(-3dB)}$	685.4 kHz	
$f_{l(\pm45°)}$	677.3 kHz	$Q = 85$
$f_{u(\pm45°)}$	685.3 kHz	

intuitive way of calculating the Q-factor of a system. Fig. 11 shows the velocity amplitude of the piezoelectric element over time.

After the vibration has reached a quasi-stationary state, the excitation frequency of 681.2 kHz is switched off and the velocity amplitude decays. The left point in Fig. 11 is selected to be at a position shortly after the excitation was switched off. The right point is defined at the position where the velocity amplitude has decayed to $1/e$ or −8.7 dB of the amplitude at the left point. Calculating the time difference between both points leads to the characteristic time τ which is 37.2 µs in the measurement above. The Q-factor can then be calculated using the relation $Q = \pi f_0 \tau$, leading to a Q-factor of 81.

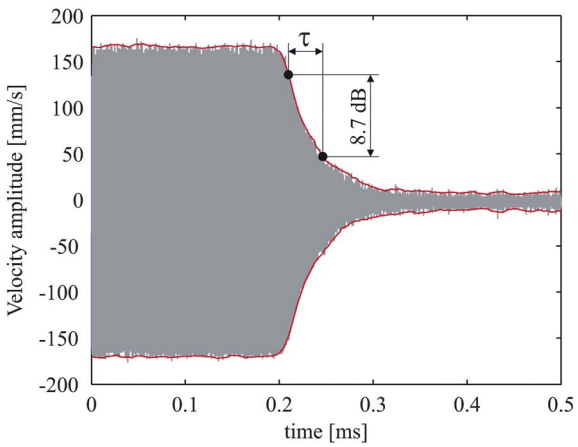

Fig. 11 Q-factor determination at the example of a thickness mode of a piezoelectric element utilizing the characteristic time of the decaying velocity amplitude. The envelope of the velocity measurement shows an exponential decay after the resonant excitation has stopped. The velocity measurement was done by laser interferometry.

2. Characterization of manipulation devices

Here a planar resonator is used to show the relation between admittance measurements and resonances in the fluid cavity. The planar resonator consists of the following five layers as shown in Fig. 12: a piezoelectric transducer (Ferroperm PZ 26, 0.5 mm), adhesive layer (Epotek H20E, 8 µm), carrier (glass, 1 mm), fluid (water, 1 mm) and reflector (glass, 0.56 mm).

The resonator is simulated with a one dimensional transfer matrix model reported in ref. 20. In Fig. 13 the admittance measurement and simulation are plotted *vs.* frequency. The fundamental resonance frequency of the piezoelectric transducer alone would be at 4.2 MHz. The peaks marked with F represent the resonances dominated by the fluid. For example the first peaks at 2.26 MHz and 2.97 MHz correspond to 1.5 and 2 wavelengths in the fluid layer and therefore 3 and 4 nodal pressure planes, respectively.

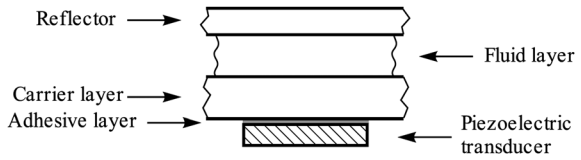

Fig. 12 Schematic view of a planar resonator consisting of the following 5 layers: piezoelectric transducer, adhesive layer, carrier, fluid and reflector, with thicknesses of 0.5 mm, 8 μm, 1 mm, 1 mm and 0.56 mm, respectively.

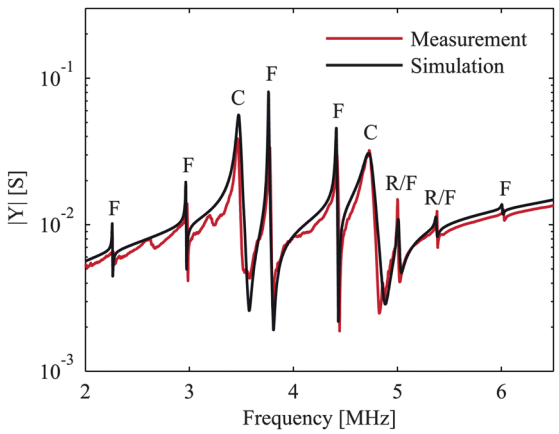

Fig. 13 Admittance measurement and simulation for a planar resonator. The model allows each of the peaks to be assigned to the corresponding layer which dominates the resonance. The peaks marked with *F* correspond to fluid resonances, *C* to carrier resonances and *R*/*F* to a combination of reflector and fluid resonances.

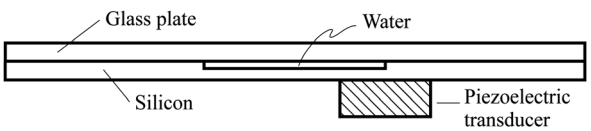

Fig. 14 Schematic view of a microfluidic device excited with a piezoelectric transducer.

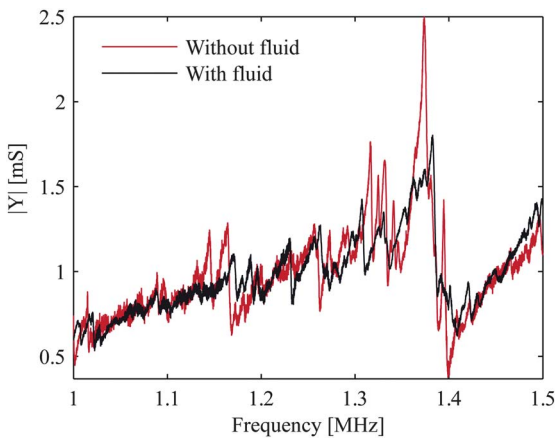

Fig. 15 Admittance plot of a piezoelectric element which was mounted on a microfabricated device. The red curve represents the measurement without fluid (air filled cavity) and the black curve represents the measurement with a fluid (water) filled cavity.

The resonant layers are determined with the transfer matrix model by plotting the pressure distribution for the different layers or by varying the layer thickness of the resonant layer in the model and observing the frequency shift of the peak in the admittance curve. The peaks *C* are dominated by a resonance in the carrier and *R*/*F* is a combination of a reflector and fluid resonance. The knowledge of which peak corresponds to which layer is important for the operation of the device. It is possible to drive the system exactly at one of the fluid resonances. When conditions like temperature are changing, also the resonance frequency will change and so will the peak in the admittance plot.

As a further example, the admittance curve of a typical microfabricated device (see Fig. 14) is measured. The main part is a 16 mm × 16 mm silicon substrate (thickness 500 μm) where a 5 mm × 6 mm cavity is etched 200 μm deep inside. The cavity is covered with a glass plate (thickness 500 μm) by anodic bonding. The actuation is done with a 6 mm × 2.5 mm piezoelectric transducer (thickness 1 mm) glued at the bottom of the device.

The admittance curve of the mounted piezoelectric element is measured for an air-filled as well as a water-filled chamber and is shown in Fig. 15. Contrary to the previous simple examples, the complex structure results in a large number of peaks in the admittance curve which are caused by additional structural resonance modes. The peaks in the admittance curve are generally less pronounced for the water-filled device, as the water causes additional damping. The determination of resonance modes by means of the admittance curve is less obvious in these complex systems, however *e.g.* the peak in the admittance curve at 1.42 MHz was found to result in a resonance where 10 lines of particles are formed in the chamber.

In addition to the shown admittance measurements, the dynamic behaviour of manipulation devices can also be measured by laser vibrometry. This tool is especially useful for the validation of FEM simulations. An example for a 1D measurement is reported in ref. 18 as shown in Fig. 16. The measurement in Fig. 16(b) shows the vertical displacement on the underside of a piezoelectric

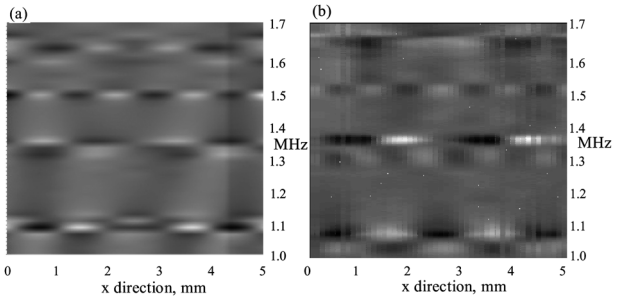

Fig. 16 Vertical displacement along a line on the underside of a piezo-electric element which was mounted on a microfabricated device. The simulation results (a) can be compared to measurements by laser interferometry (b). Reprinted from ref. 18 with permission by Elsevier.

element, which was mounted on a microfabricated device. The measurement along a line on the piezoelectric element is plotted over a frequency range of 1.0–1.7 MHz after a FFT. The frequencies at which the device is operated in resonance can be observed as well as the number of wavelengths along the measured line. The measurement is in good agreement with the simulation results shown in Fig. 16(a). Finally, an example of scanning laser vibrometry is outlined in ref. 22, where the mode shape of a piezoelectric element was measured in 2D.

E Conclusions

In this paper a number of techniques have been shown and applied, which can be used to characterize devices used for ultrasonic manipulation. The mechanical behaviour is best studied using laser interferometers with either displacement or velocity decoders. The electrical characteristics of the piezoelectric elements also give information about resonance frequencies where strong electromechanical coupling occurs. The total Q factor is a measure of how efficiently energy can be used for the manipulation. The higher the Q factor, the lower the required voltages. On the other hand, a high Q results in narrow bandwidth, which in turn might pose some difficulties in stabilizing the operation, when the temperature and therefore the resonance frequency changes. Several methods have therefore been demonstrated to determine the Q based on various measured quantities. When the device is filled with a fluid, Q will be decreased, as additional damping mechanisms are introduced. This will lower the amplitudes generated and therefore also the forces acting on particles in the fluid.

References

1 W. T. Coakley, D. W. Bardsley, M. A. Grundy, F. Zamani and D. J. Clarke, *J. Chem. Technol. Biotechnol.*, 1989, **44**, 43.
2 N. R. Harris, M. Hill, S. Beeby, Y. Shen, N. M. White, J. J. Hawkes and W. T. Coakley, *Sens. Actuators, B*, 2003, **95**, 425.
3 A. Nilsson, F. Petersson, H. Jonsson and T. Laurell, *Lab Chip*, 2004, **4**(2), 131.
4 A. Haake and J. Dual, *Ultrasonics*, 2004, **42**, 75.
5 J. Friend and L. Y. Yeo, *Rev. Mod. Phys.*, 2011, **83**, 647.
6 R. Barnkob, P. Augustsson, T. Laurell and H. Bruus, *Lab Chip*, 2010, **10**, 563.
7 J. F. Spengler, M. Jekel, K. T. Christensen, R. J. Adrian, J. J. Hawkes and W. T. Coakley, *Bioseparation*, 2000, **9**, 329.
8 M. Bass, *Handbook of Optics*, McGraw-Hill, vol. 1, 1995.
9 M. Bass, *Handbook of Optics*, McGraw-Hill, vol. 2, 1995.
10 J. Dual, M. Hageli, M. R. Pfaffinger and J. Vollmann, *Ultrasonics*, 1996, **34**, 291.
11 J. W. Wagner, Optical Detection of Ultrasound, *Physical Acoustics XIX*, Academic Press, 1990, p. 201.
12 I. N. Sneddon, *Fourier Transforms*, McGraw-Hill, 1951.
13 E. O. Brigham, *The Fast Fourier Transform*, Prentice Hall, 1974.
14 J. S. Bendat and A. G. Piersol, *Random Data: Analysis and Measurement Procedures*, Wiley-Interscience, New York, 1971.
15 J. Dual and D. Möller, *Lab Chip*, 2012, **12**, 506.
16 J. Dual and T. Schwarz, *Lab Chip*, 2012, **12**, 244.
17 D. J. Ewins, *Modal Testing: Theory and Practice*, Research Studies Press, John Wiley, 1995.
18 A. Neild, S. Oberti and J. Dual, *Sens. Actuators, B*, 2007, **121**, 452.
19 Ferroperm Piezoceramics A/S, http://www.ferroperm-piezo.com/.
20 M. Gröschl, *Acustica*, 1998, **84**, 432.
21 A. V. Mezheritsky, *Ieee Uffc*, 2005, **52**, 2120.
22 S. Oberti, A. Neild and J. Dual, *J. Acoust. Soc. Am.*, 2007, **121**, 778.

